Transport of neutral and charged nano rods across varying-section channels

Paolo Malgaretti[1,2,*] and Jens Harting[3,4]

[1] *Max-Planck-Institut für Intelligente Systeme, Heisenbergstr. 3, D-70569 Stuttgart, Germany*
[2] *IV. Institut für Theoretische Physik, Universität Stuttgart, Pfaffenwaldring 57, D-70569 Stuttgart, Germany*
[3] *Helmholtz Institute Erlangen-Nürnberg for Renewable Energy (IEK-11), Forschungszentrum Jülich, Fürther Straße 248, 90429 Nürnberg, Germany*
[4] *Department of Applied Physics, Eindhoven University of Technology, P.O. box 513, NL-5600MB Eindhoven, The Netherlands*

We study the dynamics of neutral and charged rods embedded in varying-section channels. By means of suitable approximations we derive the dependence of the local diffusion coefficient on both the geometry and charge of the rods. This microscopic insight allows us to provide predictions for the permeability of varying-section channel to rods with diverse lengths, aspect ratios and charge. Our analysis show that the dynamics of charge rods is quite sensitive to the geometry of the channel and that their transport can be controlled by tuning both the shape of the confining walls and the charge of the rod. Interestingly, we found that the channel permeability does not depend monotonically on the charge of the rod. This highlight the chance of novel mechanisms to separate charged rods.

I. INTRODUCTION

The transport of molecules, proteins and small particles across pores, channels and, in general, porous materials is of paramount relevance in several biological, environmental and technological scenarios. In biology, ions [1, 2] and molecules are transported across membrane pores, RNA is transported across the nuclear membrane [3, 4] and the crowded environment of cell cytoplasm provide dynamical obstacles to the motion of organelles and vesicles [5]. Similarly, in environmental sciences, pollutants and plant nutrients spread across the porous matrix of rocks and soil. Finally, in recent years the development of experimental techniques such as DNA sequencing [6] and resistive-pulse sensing techniques [7–10] have been developed by exploiting transport across pores.

On the theoretical side, tackling these problems is typically complicated since it requires detailed numerical simulations that take into account the interactions between the suspended object and the confining walls. Recently, several groups have contributed developing the so-called Fick-Jacobs approximation[11–15]. This scheme relies on the assumption that when the net longitudinal velocity is slow enough, the transported object will explore the directions transverse to the motion with a probability distribution that is very close to the equilibrium one. Thanks to this approximation, the geometry of the pore as well as the interaction with the walls can be accounted for by the local equilibrium free energy. Interestingly such an approach has been shown to be quite reliable for the transport of colloids [16, 17], ions [18–21], and polymers [22–24] just to mention a few among others (see recent review articles [25, 26] for a more comprehensive list).

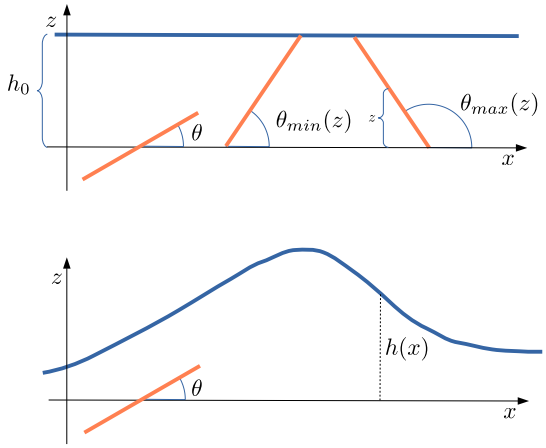

FIG. 1. Top: scheme of a rod in a plane channel. Bottom: a rod in a varying-section channel

In this article we study the dynamics of charged rods confined in varying section channels. In particular, we propose an extension of the Fick-Jacobs approximation that allows us to account for both the geometry of the rod as well as for its net charge, First we have tested our approach against known experimental results [27] for neutrally charged rods. Interestingly, our model retrieves both the local dependence of the diffusion coefficient as well as the dependence of the Mean First Passage Time profile. Second, we have used our model to predict the dependence of the diffusion coefficient on the geometry of both the channel and the rod as well as on the charge of the rod. For neutrally charged rods, in agreement with Ref. [27], we found that the local diffusion coefficient is maximum at the channel bottleneck, i.e. where the rod is mainly oriented along the channel axes. Interestingly, we found that the modulation of the local diffusion coefficient is maximized when the length of the rod major axis is comparable to the channel average section and it becomes vanishing small when these two length scales

* Corresponding Author: malgaretti@is.mpg.de

differ. Moreover, our data show that the net diffusion in a varying section channel can be enhanced as compared to the case of a Interestingly we found that that such a modulation can be even amplified by the electrostatic interaction between the rod and the channel walls.

II. MODEL

We characterize the transport of rigid rods across a $2D$ varying-section channel whose half-section is given by

$$h(x) = h_0 \left(1 - h_1 \cos\left(\frac{2\pi}{L_0}x\right)\right) \tag{1}$$

Accordingly the $2D$-Smoluchowski equation reads:

$$\partial_t \rho(x,z,\theta,t) = \partial_x J_x + \partial_z J_z + \partial_\theta J_\theta \tag{2}$$

with

$$J_x = \mathbf{e}_x \cdot \mathbf{D}(\theta) \cdot \left[\bar{\nabla}\rho + \rho\beta\bar{\nabla}W\right] \tag{3}$$
$$J_z = \mathbf{e}_z \cdot \mathbf{D}(\theta) \cdot \left[\bar{\nabla}\rho + \rho\beta\bar{\nabla}W\right] \tag{4}$$
$$J_\theta = D_\theta \partial_\theta \rho \tag{5}$$

where $\mathbf{D}$ is the translational diffusion matrix that accounts for the fact that the diffusion along the major axis of the rod differs from that perpendicular to it , D_θ is the rotational diffusion coefficient and W accounts for the conservative forces acting on the rod.

In the following we assume that translation along the channel axis is slow enough such that ρ retains its equilibrium profiles along z and θ, i.e. we assume that we have

$$J_z = 0 \tag{6}$$
$$J_\theta = 0 \tag{7}$$

This implies that , i.e.

$$\rho(x,z,\theta,t) = p(x,t) g_{z\theta}(x,z.\theta) \tag{8}$$
$$g_{z\theta}(x,z,t) = \frac{e^{-\beta W(x,z,\theta)}}{e^{-\beta A(x)}} \tag{9}$$
$$e^{-\beta A(x)} = \frac{1}{2\pi h_0}\int_0^\pi \int_{-\infty}^{\infty} e^{-\beta W(x,z,\theta)} dz d\theta \tag{10}$$
$$J_x = \mathbf{e}_x \cdot \mathbf{D}(\theta) \cdot \mathbf{e}_x \left[\partial_x \rho + \rho\beta\partial_x W\right] \tag{11}$$

Integrating in $d\theta$ and using Eq.(6) we have:

$$\partial_x \int_0^\pi \int_{-\infty}^{\infty} \mathbf{e}_x \cdot \mathbf{D}(\theta) \cdot \mathbf{e}_x \left[\partial_x \rho + \rho\beta\partial_x W\right] dz d\theta = \partial_x \left[\mathcal{D}(x)\left(\partial_x p + p\beta\partial_x A\right)\right] \tag{12}$$

where

$$\mathcal{D}(x) = \frac{1}{2\pi h_0}\int_0^\pi \int_{-\infty}^{\infty} \mathbf{e}_x \cdot \mathbf{D}(\theta) \cdot \mathbf{e}_x \frac{e^{-\beta W(x,z,\theta)}}{e^{-\beta A(x)}} dz d\theta \tag{13}$$

is the effective *local* diffusion coefficient and

$$A(x) = -fx - k_B T \ln\left[\int_{-\infty}^{\infty} e^{-\beta W(x,y)} dy\right] \tag{14}$$

is the potential of mean force. Accordingly, Eqs.(12),(2) can be rewritten as:

$$\partial_t p(x,t) = -\partial_x \left\{\mathcal{D}(x)\left[\partial_x p(x,t) + \beta p(x,t)\partial_x A(x)\right]\right\} \tag{15}$$

The stead-state solution of Eq.(15) reads:

$$p(x) = e^{-\beta A(x)}\left[J\int_0^x \frac{e^{\beta A(x')}}{\mathcal{D}(x')} dx' + \Pi\right] \tag{16}$$

For periodic boundary conditions and imposing the normalization of the probability we obtain:

$$\Pi = -J\frac{\int_0^L \frac{e^{\beta A(x)}}{\mathcal{D}(x)} dx}{e^{-\beta(A(0)-A(L))} - 1} \tag{17}$$
$$J = -\left[\int_0^L e^{-\beta A(x)}\left[\int_0^x \frac{e^{\beta A(x')}}{\mathcal{D}(x')} dx' + \Pi_0\right] dx\right]^{-1} \tag{18}$$

In the frame of reference of the rod we have

$$\mathbf{D} = D_0 \begin{bmatrix} \frac{l}{L} & 0 \\ 0 & 1 \end{bmatrix} \tag{19}$$

where $D_0 \frac{l}{L}$ is the diffusion coefficient along the minor axis of the rod, $\mathbf{e}_\perp$, and D_0 is the diffusion coefficient along the major axis of the rod, $\mathbf{e}_\parallel$. According to Fig.1 we have that $\mathbf{e}_x = \cos\theta \mathbf{e}_\parallel - \sin\theta \mathbf{e}_\perp$. This leads to the following expression for the local diffusion coefficient:

$$\mathbf{e}_x \cdot \mathbf{D}(\theta) \cdot \mathbf{e}_x = D_0\left(\cos^2\theta + \frac{l}{L}\sin^2\theta\right) \tag{20}$$

that, once substituted into Eq.(13),

$$\mathcal{D}(x) = \frac{D_0}{2\pi h_0}\int_0^\pi \int_{-\infty}^{\infty}\left(\cos^2\theta + \frac{l}{L}\sin^2\theta\right)\frac{e^{-\beta W(x,z,\theta)}}{e^{-\beta A(x)}} dz d\theta \tag{21}$$

III. RESULTS

A. Neutral rods

At first we focus on neutral rods. In the following, we focus on the case in which the local radius of curvature is much larger than the length of the rod. In such a regime the channel walls can be approximated as locally parallel to the longitudinal axis. Accordingly we have that the potential W reads:

$$W(x,z) = \begin{cases} -fx & |z| < h(x)\,\&\,\theta_{min} < \theta < \theta_{max} \\ \infty & else \end{cases} \tag{22}$$

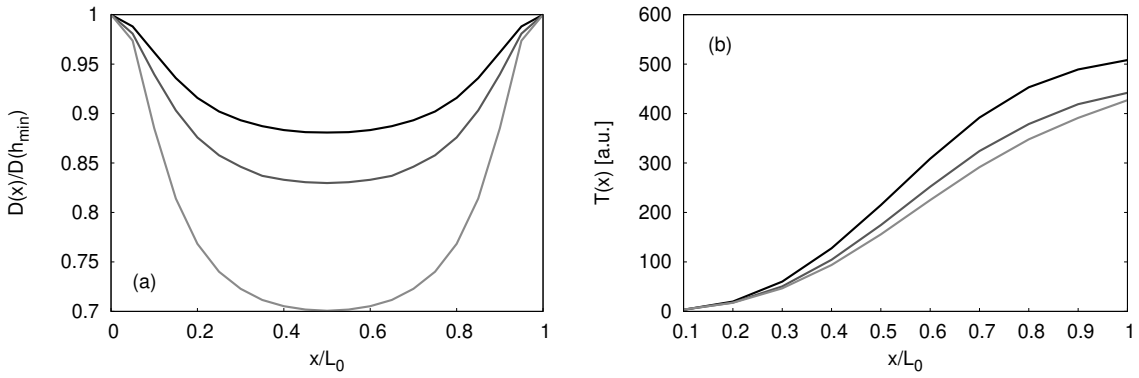

FIG. 2. Check of the model against experimental data. (a): Dependence of the diffusion coefficient $\mathcal{D}(x)$ normalized by the value at the bottleneck. In order to check the validity of the model the values of the parameters have been chosen to be close to those used in Fig.3.a of Ref.[27]. Accordingly we have: $L = 1\mu m$, $h_0/L = 0.3$ and $L_{max}/h_0 = 0.3, 0.4, 0.53$, lighter colors stands for larger values of L_{max}. (b): Mean First Passage Time (MFPT) with reflecting boundary conditions at the origin and absorbing at x. The y axis has been rescaled to clarify the comparison with Ref.[27].

with

$$\theta_{max} = \begin{cases} \frac{\pi}{2} + \arccos\left(\frac{h(x)-z}{L}\right) & h(x) - L \leq |z| \leq h(x) \\ \pi & |z| < h(x) - L \end{cases} \tag{23}$$

$$\theta_{min} = \begin{cases} \frac{\pi}{2} - \arccos\left(\frac{h(x)-z}{L}\right) & h(x) - L \leq |z| \leq h(x) \\ 0 & |z| < h(x) - L \end{cases} \tag{24}$$

and the local free energy reads:

$$A(x) = -fx - k_B T \ln\left[\frac{2}{h_0}\int_0^{h(x)} \pi + \theta_{min}(z) - \theta_{max}(z) dz\right] \tag{25}$$

Accordingly, the effective diffusio coefficient reads

$$\mathcal{D}(x) = \frac{D_0}{2\pi h_0} \frac{\int_0^{2\pi}\int_{-h(x)}^{h(x)} \left(\cos^2\theta + \frac{l}{L}\sin^2\theta\right) \Theta\left(\theta - \theta_{min}(x,z)\right) \Theta\left(\theta_{max}(x,z) - \theta\right) dz d\theta}{\int_0^{2\pi}\int_{-h(x)}^{h(x)} \Theta\left(\theta - \theta_{min}(x,z)\right) \Theta\left(\theta_{max}(x,z) - \theta\right) dz d\theta} \tag{26}$$

where L is half-length of the major axis of the rod (see Fig.1) and Θ is the Heaviside step function. In Eqs.(23),(24) we have assumed that the aspect ratio between the long axis, L, and the minor axis, l, is such that $L/l \ll 1$ and hence we can disregard the geometric corrections to Eqs.(23),(24) due to the finiteness of l.

1. *Diffusion*

At first we have compared our analytical predictions for the diffusion coefficient against experimental results. As shown in Fig.2.a we see that the agreement between the predictions of Eq.(26) and the data from Ref.[27] is quite good. Once the agreement for the diffusion coefficient as been assessed we focus on the validity of the Fick-Jacobs approximation. In order to check this we compute the Mean First Passage Time (MFPT) between the origin and an arbitrary position x:

$$T(x) = \int_0^x dx e^{\beta A(x')} \int_0^{x'} \frac{e^{-\beta A(z)}}{\mathcal{D}(z)} dz \tag{27}$$

Interestingly, the predictions of Eq.(27) match well with the data reported in Ref.[27].

As already shown in Ref.[27] the diffusion coefficient is maximum at the channel bottleneck where the rod is mainly parallel to the axis of the channel. Next we have studied the dependence of the ratio between the maximum and the minimum local diffusion coefficients on the length of the rod. As expected, Fig.3 shoes that in the asymptotic limits, $L/h_0 \ll 1$ and $L/h_0 \gg 1$ the ratio is close to one, namely the diffusion coefficient shows a very mild dependence on the position. In contrast, for $L \simeq h_0$, Fig.3.a shows that increasing the corrugation of the channel increases the range of values of the rod length for which the local diffusion coefficients is sensitive to the local channel section. Clearly if the aspect ratio, L/l approaches unity the diffusion coefficients becomes homogeneous along the channel. Fig.3.b shows that the local diffusion coefficient, as a function of the aspect ratio, attains an asymptotic value already for $\frac{L}{l} \sim 10$.

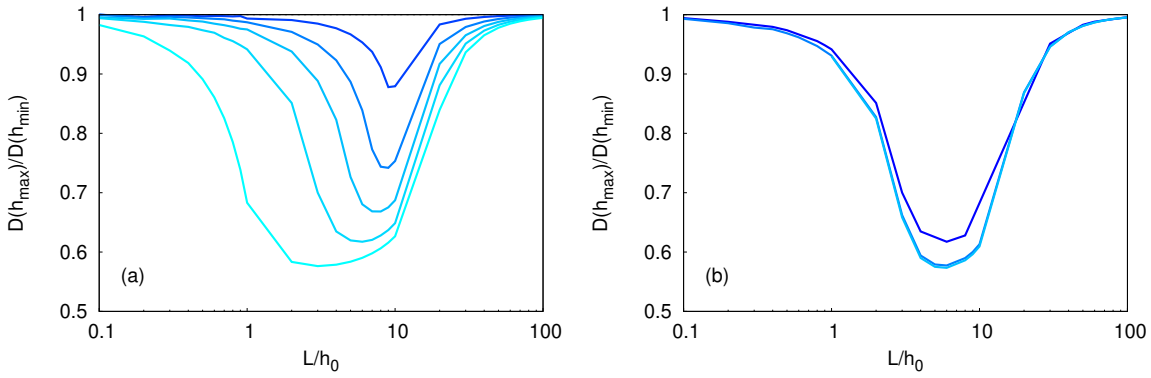

FIG. 3. Diffusion. Top: ratio of the effective diffusion coefficient at the maximum channel amplitude and at the bottleneck for rods with fixed aspect ratio $L_{min}/L_{max} = 0.1$ as a function of L_{max} and for different values of $h_1/h_0 = 0.1, 0.3, 0.5, 0.7, 0.9$ standing lighter colors for larger values of h_1. Bottom: ratio of the effective diffusion coefficient at the maximum channel amplitude and at the bottleneck for different aspect ratio: $L_{min}/L_{max} = 0.001, 0.01, 0.1$ and $h_1/h_0 = 0.7$. Lighter colors stands for larger values of the aspect ratio L/l.

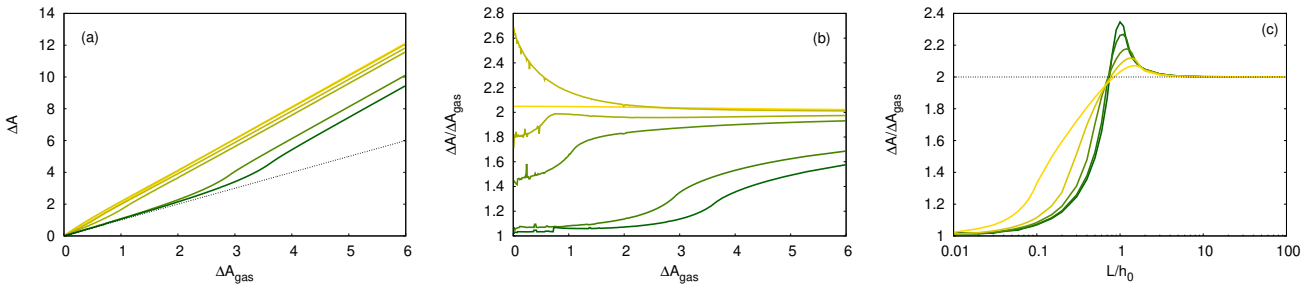

FIG. 4. Equilibrium free energy barrier. Top and center: dependence of the free energy barrier for a rod of different length $l/h0 = 0.05, 0.1, 0.5, 0.7, 1, 2$ (from green to yellow) as a function of the free energy barrier of the ideal gas. Bottom: Dependence of the free energy barrier on the length, l, of the rod for different channel corrugations $\Delta S_{gas} \simeq 0.4, 0.6, 1.1, 1.7, 3$

2. *Free energy barrier*

Having an explicit formula for the free energy, it allows us to discuss the dependence of the equilibrium ($f = 0$) free energy barrier defined as the difference between the free energy at the bottleneck and the one at the channel widest section:

$$\Delta A = A(h_{min}) - A(h_{max}) \tag{28}$$

For comparison we recall that the free energy different for an ideal gas depends solely on the geometry of the channel:

$$\Delta A_{gas} = \ln\left[\frac{h_{max}}{h_{min}}\right] \tag{29}$$

Interestingly we found that the dependence of the free energy barrier of rods strongly depends on their length. Indeed, while for shorter rods, $L/h_0 \lesssim 0.5$ the free energy barrier of the rod increases upon increasing channel corrugation (i.e. increasing ΔA_{gas}) for longer rods, $l/h_0 \gtrsim 1$ the free energy barrier of the rod decreases upon increasing ΔA_{gas}, as shown in Fig.4. Additionally we found that, for every geometry of the channel, the maximum departure of ΔA from ΔA_{gas} is obtained when the length of the rod is comparable to the channel average section, $L \simeq h_0$. Interestingly, for rods much longer than the channel section we have that $\Delta A \to 2\Delta A_{gas}$. In order to understand this asymptot we can expand Eq.(25) for the argument of the arccos close to zero. Accordingly we obtain that $A(x) \propto 2\ln[h(x)]$ that eventually leads to $\Delta A/\Delta A_{gas} \to 2$.

3. *Transport*

Next, we analyze the transport of rods under the action of a constant force. In order to simplify the analysis we assume that the fluid keeps at rest, i.e. there is no advection of rods due to fluid motion. To this regard it results insightful to look at the channel permeability:

$$\mu = \frac{JL_0}{\beta\bar{\mathcal{D}}(L)f} \tag{30}$$

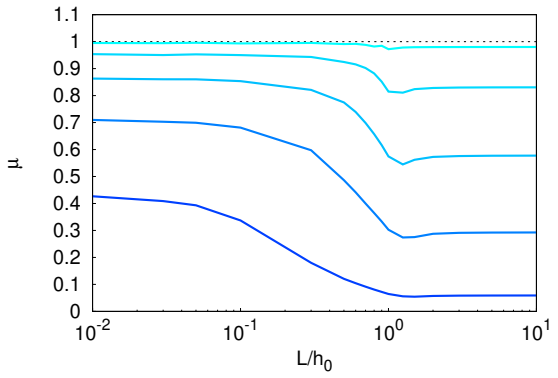

FIG. 5. Flux, J, as a function of the rod length, L for rods with fixed aspect ratio, $L/l = 100$ and for different values of $h_1/h_0 = 0, 0.1, 0.3, 0.5, 0.7, 0.9$.

where

$$\bar{\mathcal{D}}(L) = \frac{1}{L}\int_0^L \mathcal{D}(x,L)dx \tag{31}$$

is the diffusion coefficient averaged over the channel period, L. Interestingly Fig.5 shows that the dependence of μ on the length of the major axis of the rod, L, is non-monotonous and it shows a (weak) minimum.This behavior is similar to that of polymers confined between corrugated plates (see Ref. [22]).

B. Charged rods

Next we analyze the case of charged rods. For simplicity we assume that the charge, ze, is localized at the center of the rod and that the channel walls are characterized by a constant charge density, σ. In addition, we assume that a dilute monovalent electrolyte is suspended in the fluid phase so that the system is electrically neutral. In this regards, the rod brings an extra charge, whose magnitude is assumed to be smaller than that of the charge of the double layer. Accordingly we have that the electrostatic potential inside the channel reads:

$$\phi = \frac{\sigma}{\varepsilon\kappa}\frac{\cosh(\kappa z)}{\sinh(\kappa h(x))} = \phi_0\frac{1}{\kappa h_0}\frac{\cosh(\kappa z)}{\sinh(\kappa h(x))} \tag{32}$$

with $\phi_0 = \sigma h_0/\epsilon$. The local free energy becomes

$$A(x) = -fzex - k_BT\ln\left[\frac{2}{h_0}\int_0^{h(x)} e^{-\beta q\phi_0\frac{\cosh(\kappa z)}{\sinh(\kappa h(x))}}\left(\pi - 2\arccos\left(\frac{h(x)-z}{L}\right)\right)dz\right] \tag{33}$$

where $\phi_0 = \frac{\sigma}{\varepsilon\kappa}$ and q is the charge of the rod and the diffusion coefficient reads:

$$\mathcal{D}(x) = \frac{D_0}{2\pi h_0}\frac{\int_0^{2\pi}\int_{-h(x)}^{h(x)}\left(\cos^2\theta + \frac{l}{L}\sin^2\theta\right)e^{-\beta q\phi_0\frac{\cosh(\kappa z)}{\sinh(\kappa h(x))}}\Theta\left(\theta-\theta_{min}(x,z)\right)\Theta\left(\theta_{max}(x,z)-\theta\right)dzd\theta}{\int_0^{2\pi}\int_{-h(x)}^{h(x)}\Theta\left(\theta-\theta_{min}(x,z)\right)\Theta\left(\theta_{max}(x,z)-\theta\right)dzd\theta} \tag{34}$$

and that the magnitude of the external force is not depending on the value of the charge, ze. The dependence of the channel permeability is shown in Fig.6. In particular, fig.6.a shows that the dependence of μ on the charge of the rod is non-monotonous. When the magnitude of the charge is very large (for both sign of the charge) the permeability becomes vanishing small. Indeed, for such case the effective energy barrier to be overcome is very large and hence μ becomes very small. In contrast, upon reducing the magnitude of the charge μ increases at it reaches its maximum for weakly negatively charged rods, i.e. when rods are *attracted* by the channel walls. As shown in fig.6.a the optimal value of the charge depends on the channel corrugation and it decreases upon increasing the channel corrugation. Fig.6.b shows the dependence of μ on the channel corrugation, encoded in ΔA_{gas}, for diverse values of the charge of the rod. Interestingly, we notice that for positively charge rods, i.e. repelled from the channel walls, μ is hampered as compared to the neutral charge case. In contrast, negatively charged rods, hence attracted by the channel walls, experience an enhanced permeability as compared to the neutral charged ones. This scenario is persists for all rod lengths we have investigated. Fig.6.c shows that the dependence of μ on the length of the rod is similar to that of neutrally charged rods, given the enhancement (reduction) factor for negatively (positively) charge rods that we have discussed above. Finally we have studied the dependence of the flux of charged rods as a function of the Debye length. Interestingly, fig.6.d shows that the flux of negatively charged rods (hence attracted by the channel walls) has a non-monotonous dependence on the dimensionless inverse Debye length κh_0 and it displays a maximum around $\kappa h_0 \lesssim 1$ for all the geometries of the channel that we have explored. In contrast, the net flow of positively charged rods increases monotonously with the inverse Debye length κh_0.

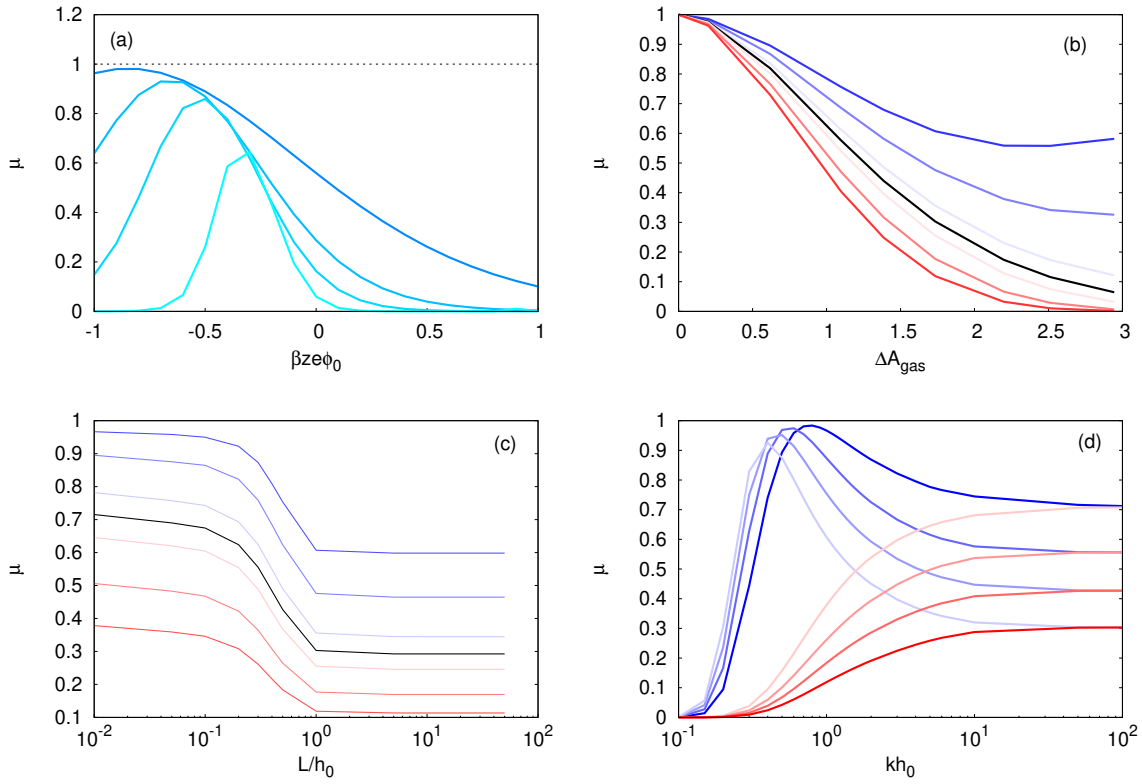

FIG. 6. Channel permeability to charged rods. (a): μ as a function of $\beta ze\phi_0$ for different values of the channel corrugation, $h_1/h_0 = 0.5, 0.7, 0.8, 0.9$, with $\kappa h_0 = 1$. Lighter colors stand for larger values of h_1. The force is proportional to the charge and, for a unit charge it amounts to $\beta f z e L = 0.1$. (b): μ as a function of the channel corrugation encoded in ΔA_{gas} for $\kappa h_0 = 1$, $L/h_0 = 1$, $L/l = 100$ and for different values of the wall potential, $\beta ze\phi_0 = -0.5, -0.3, -0.2, -0.1$, in blue colors lighter colors stands for smaller magnitudes of the charge, $\beta ze\phi_0 = 0$, in black and $\beta ze\phi_0 = 0, 0.1, 0.3, 0.5$ in red colors lighter colors stands for smaller magnitudes of the wall potential. (c): μ as a function of the length of the major axis of the rod, L, normalized by h_0 for $\kappa h_0 = 1$, $h_1 = 0.7$, $L/l = 100$ and for different values of the wall potential, $\beta ze\phi_0 = -0.5, -0.3, -0.1, 0, 0.1, 0.3, 0.5$, that is color coded: blue (red) lines stand for negative (positive) charges and lighter colors stands for smaller magnitudes of the wall potential. The black solid line stands for $z = 0$. (d): μ as a function of κh_0 for $h_1 = 0.7$, $L/l = 100$ and for $\beta ze\phi_0 = -0.5$ (blue lines) and $\beta ze\phi_0 = 0.5$ (red lines). In blue colors lighter colors stands for larger values of $L/h_0 = 0.01, 0.3, 0.5, 1$ and $\beta ze\phi_0 = 0.5$ in red colors lighter colors stands for larger values of $L/h_0 = 0.01, 0.3, 0.5, 1$.

C. Conclusions

We have studied the dynamics of charged rods embedded in varying-section channels. Under the assumption of slowly varying channel sections, $\partial_x h(x) \ll 1$ we have extended the Fick-Jacobs approximation to the case of charged rods. Our approximation allows us to derive an expression for the local diffusion coefficient, $\mathcal{D}(x)$ (see Eq.(21)). We have tested our prediction for the case of neutrally charged rods against experimental results (see Ref.[27]). Interestingly our predictions (see Fig.2) match very well with the experimental data for what concern both the local diffusion coefficient as well as for the Mean First Passage Time. We remark that, while in experiments hydrodynamic coupling between the rods and the channel walls is naturally accounted for, it is not so in our model. Hence a first results of our analysis is that, in the regime under study, hydrodynamic coupling plays a minor role in the diffusion of rods within corrugated channels. In order to grasp the relevance of the rod geometry on the free energy barrier, Δ, we have compared it to that of point particles, ΔA_{gas}. Interestingly, we found that the enhancement in the free energy difference, ΔA, is at most twofold (see Fig.4).c. Next we have characterized the channel permeability, μ, to neutral rods as a function of their length. As expected we found that μ is hampered for long rods as compared to shorter ones (see Fig.5). Finally, we have characterized the channel permeability to charged rods. In particular we have focused on the dependence of μ on the rod size and charge. Interestingly, Fig.6.a shows that μ has a non-monotonous dependence on the rod charge. Hence the channel geometry can be used to select rods with a desired length. Next we have further characterized the dependence of μ on other parameters such as the geometry of the channel (see Fig.6.b), the length of the rod (see Fig.6.c) and the inverse Debye length κ (see Fig.6.d). Our results show

that μ can be tuned by properly combining the channel geometry and the length and charge of the rod.

[1] C. Calero, J. Faraudo, and M. Aguilella-Arzo, Phys. Rev. E **83**, 021908 (2011).
[2] A. Peyser, D. Gillespie, R. Roth, and W. Nonner, Biophysical Journal **107**, 1841 (2014).
[3] D. V. Melnikov, Z. K. Hulings, and M. E. Gracheva, Physical Review E **95**, 063105 (2017).
[4] P. Bacchin, Membranes **8**, 10 (2018).
[5] B. Alberts, A. Johnson, J. Lewis, M. Raff, K. Roberts, and P. Walter, *Molecular Biology of the Cell* (Garland Science, Oxford, 2007).
[6] D. J. Bonthuis, C. Meyer, D. Stein, and C. Dekker, Physical review letters **101**, 108303 (2008).
[7] O. A. Saleh and L. L. Sohn, Proc. Natl. Acad. Sci. U. S. A. **100**, 820 (2003).
[8] T. Ito, L. Sun, M. A. Bevan, and R. M. Crooks, **20**, 6940 (2004).
[9] E. A. Heins, Z. S. Siwy, L. A. Baker, and R. C. Martin, Nano Lett. **5**, 1824 (2005).
[10] N. Arjmandi, W. Van Roy, L. L., and G. Borghs, Anal. Chem. **84**, 8490 (2012).
[11] R. Zwanzig, J. Phys. Chem. **96**, 3926 (1992).
[12] D. Reguera and J. M. Rubi, Phys. Rev. E **64**, 061106 (2001).
[13] P. Kalinay and J. K. Percus, Phys. Rev. E **78**, 021103 (2008).
[14] S. Martens, G. Schmidt, L. Schimansky-Geier, and P. Hänggi, Phys. Rev. E **94**, 2492 (2011).
[15] G. Chacón-Acosta, I. Pineda, and L. Dagdug, J. Chem. Phys. **139**, 214115 (2013).
[16] D. Reguera, G. Schmid, P. S. Burada, J. M. Rubi, P. Reimann, and P. Hänggi, Phys. Rev. Lett. **96**, 130603 (2006).
[17] D. Reguera, A. Luque, P. S. Burada, G. Schmid, J. M. Rubi, and P. Hänggi, Phys. Rev. Lett. **108**, 020604 (2012).
[18] P. Malgaretti, I. Pagonabarraga, and J. M. Rubi, Phys. Rev. Lett **113**, 128301 (2014).
[19] P. Malgaretti, I. Pagonabarraga, and J. M. Rubi, Macromol. Symposia **357**, 178 (2015).
[20] P. Malgaretti, I. Pagonabarraga, and J. M. Rubi, Macromol. Symposia **357**, 178 (2015).
[21] M. Chinappi and P. Malgaretti, Soft Matter **14**, 9083 (2018).
[22] V. Bianco and P. Malgaretti, The Journal of Chemical Physics **145**, 114904 (2016).
[23] P. Malgaretti and G. Oshanin, Polymers **11** (2019), 10.3390/polym11020251.
[24] I. V. Bodrenko, S. Salis, S. Acosta-Gutierrez, and M. Ceccarelli, The Journal of Chemical Physics **150**, 211102 (2019).
[25] P. S. Burada, P. Hänggi, F. Marchesoni, G. Schmid, and P. Talkner, ChemPhysChem **10**, 45 (2009).
[26] P. Malgaretti, I. Pagonabarraga, and J. Rubi, Frontiers in Physics **1**, 21 (2013).
[27] X. Yang, Q. Zhu, C. Liu, W. Wang, Y. Li, F. Marchesoni, P. Hänggi, and H. P. Zhang, Phys. Rev. E **99**, 020601 (2019).